

Figure 1. Generalized surface geology map of Sabine Peninsula (after Harrison, 1994) displaying sedimentary stratigraphic divisions.

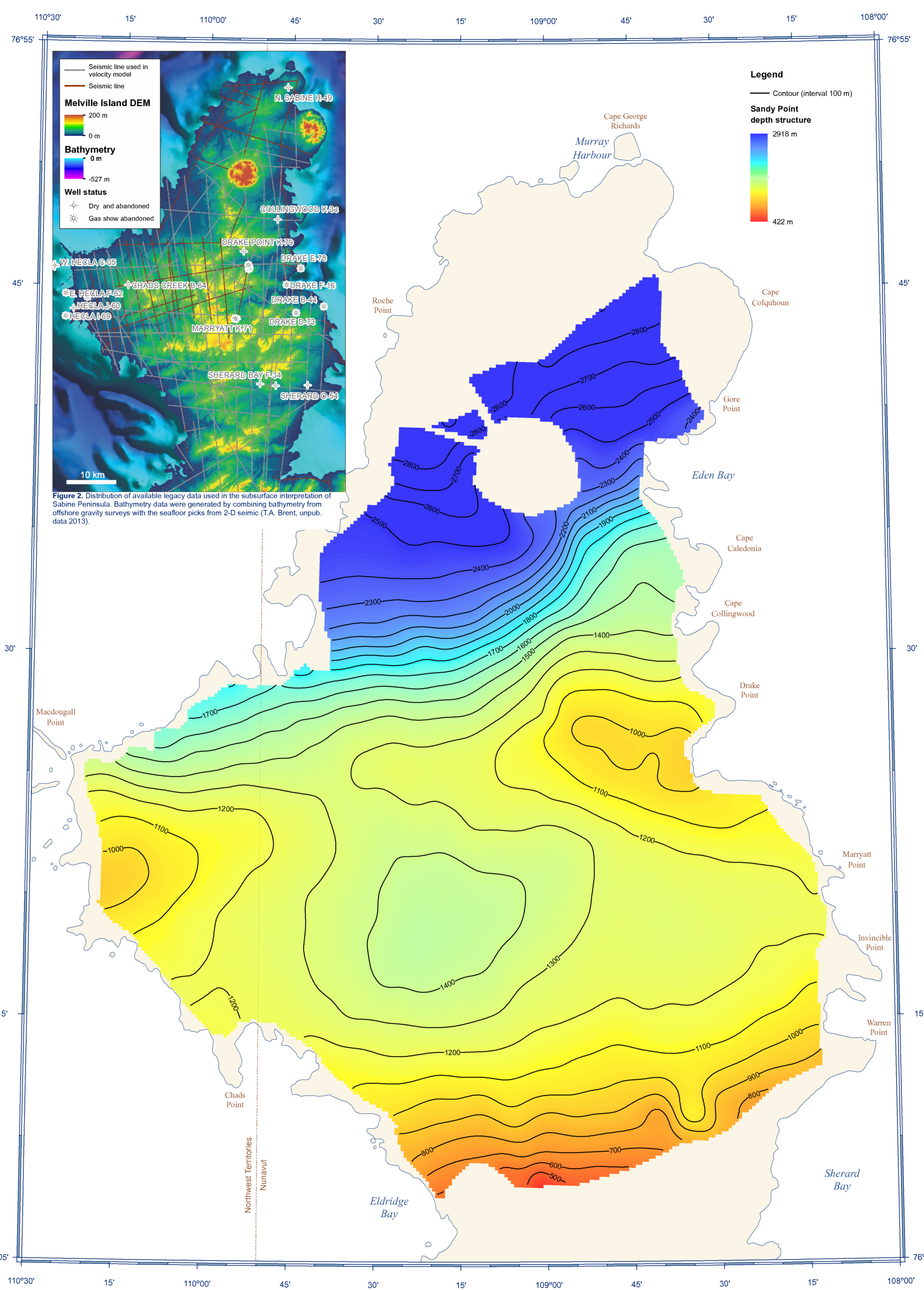


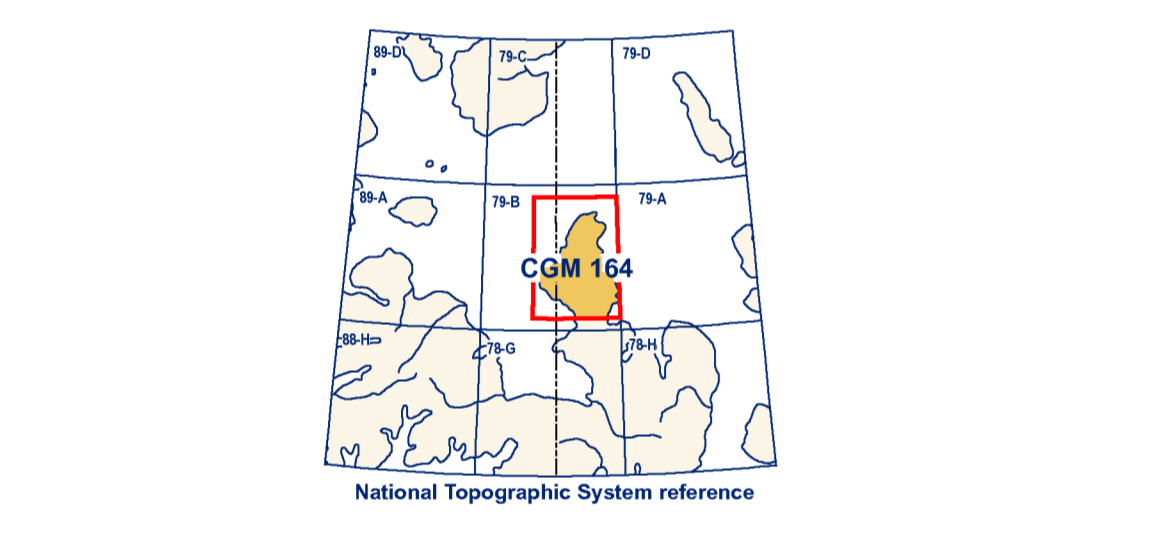
Figure 2. Distribution of available legacy data used in the subsurface interpretation of Sabine Peninsula. Bathymetry data were generated by combining bathymetry from offshore gravity surveys with the seafloor picks from 2-D seismic (T.A. Brent, unpub. data 2013).

Abstract
Sabine Peninsula of Melville Island was the subject of an oil and gas exploration boom from 1981 to 1985, during which time seismic-reflection data were collected and wells were drilled as a result of the two largest conventional natural gas fields in Canada were discovered.

Résumé
La péninsule de Sabine de l'île de Melville a connu un boom d'exploration gazière et pétrolière entre 1981-1985 pendant lequel des données de sismique-réflexion furent acquises et des puits forés. En résultat la découverte des deux plus grands champs de gaz naturel conventionnels du Canada.

Seismic-reflection methods use sound waves to image the internal structure of the Earth. Waves are emitted at the surface before being reflected back to the surface by geological interfaces and recorded. Modern analysis methods were used to re-investigate existing seismic data. In doing so, eight seismic unit boundaries identified on seismic profiles in two-way time were correlated to the regional geological framework and gridded to provide subsurface maps. Each map approximates the structures preserved at that particular time or depth allowing the enhancement of the geological knowledge of Sabine Peninsula and better delineation of elements of the petroleum systems therein.

La sismique-réflexion utilise des ondes sonores pour imaginer la structure interne de la Terre. Les ondes sont émises en surface avant d'être réfléchies de nouveau vers la surface par des interfaces géologiques où elles sont enregistrées. Des méthodes d'analyse modernes furent utilisées pour ré-investiger des données sismiques existantes. Avec huit limites d'unités sismiques identifiées sur les profils sismiques en temps de parcours aller-retour lanés combinés, au cadre géologique régional et maillées afin de produire des cartes de la sous-surface. Chaque carte est une approximation des structures préservées à un certain temps ou à une certaine profondeur nous permettant d'améliorer la connaissance géologique de la péninsule de Sabine et de mieux délimiter les éléments des systèmes pétroliers s'y trouvant.



Cover Illustration
Permian sandstone hoodoos, Sabine Peninsula, Melville Island, Nunavut. Photograph by T.A. Brent, 2013-242

Catalogue No. M163-1164-2013E-PDF
ISBN 978-1-100-29222-4
doi:10.4095/293088

© Her Majesty the Queen in Right of Canada 2013

Canadian Geoscience Maps
Natural Resources Canada / Ressources naturelles du Canada

CANADIAN GEOSCIENCE MAP 164
TIME- AND DEPTH-STRUCTURE MAP
SANDY POINT FORMATION
Sabine Peninsula, Melville Island
Nunavut-Northwest Territories
1:200 000



ess.nrcan.gc.ca
Canadian Geoscience Maps
Canada

Authors: V.I. Brake, M.J. Duchesne, K. Dewing, M. Claprood, E. Oke, and T.A. Brent
Time-structure map by: V.I. Brake and M.J. Duchesne, Geological Survey of Canada, 2013
Depth-structure map by: M.J. Duchesne and V.I. Brake, Geological Survey of Canada, 2013
Seismic interpretation by: V.I. Brake and M.J. Duchesne, Geological Survey of Canada, 2010-2013

Geomatics by: V.I. Brake, Geological Survey of Canada and G. Huot-Vézina, Institut national de la recherche scientifique
Cartography by: R. Boivin
Scientific editing by: E. Inglis
Initiative of the Geological Survey of Canada, conducted under the auspices of the Western Arctic Islands' project as part of Natural Resources Canada's Geo-mapping for Energy and Minerals (GEM) program.

CANADIAN GEOSCIENCE MAP 164
TIME- AND DEPTH-STRUCTURE MAP
SANDY POINT FORMATION
Sabine Peninsula, Melville Island
Nunavut-Northwest Territories
1:200 000

Map projection: Universal Transverse Mercator, zone 12
North American Datum 1983
Base map at the scale of 1:250 000 from Natural Resource Canada, with modifications.
Proximity to the North Magnetic Pole causes the magnetic compass to be useless in this area.

The Geological Survey of Canada welcomes corrections or additional data that may improve the accuracy of this map.
The data may include additional observations not portrayed on this map. See documentation accompanying the data.
This publication is available for free download through GEOCAN (http://geocan.ess.nrcan.gc.ca/).
This map is not to be used for navigational purposes.

DESCRIPTIVE NOTES

INTRODUCTION
The time- and depth-structure maps presented herein are part of an eight-map series of the subsurface of Sabine Peninsula spanning the Early Permian through Early Cretaceous interval. These maps are the product of the application of modern geoscientific methods of processing and interpretation to a suite of legacy seismic-reflection data from onshore Sabine Peninsula (Melville Island, Western Arctic Islands). The resulting processed seismic lines were interpreted using the existing regional geological framework (see Harrison, 1999) by integrating existing regional well data, geological logs, age control, and lithological information through synthetic seismograms.

REGIONAL SETTING
The Sabine Peninsula is located within the Sverdrup Basin in the Queen Elizabeth Islands of the western Arctic. The Sverdrup Basin extends for about 1300 km in a northeast-southwest direction and is up to 350 km wide. The basin contains up to 10 km of sedimentary strata (Embry and Beauchamp, 2008). The Sverdrup Basin is separated from the underlying Franklin Basin by an unconformity at the base of the Carboniferous strata. The Franklin Basin was extensively widespread following the Late Devonian-earliest Carboniferous Eiseismitian Orogeny. The resulting rift-related structural depression acted as a major depocentre for the Carboniferous through the Paleogene (Embry and Beauchamp, 2008). The Sverdrup Basin succession was uplifted and deformed during the early Cenozoic Eurasian Orogeny.

The surface geology of Melville Island is dominated by Lower Paleozoic strata of the Franklinian Basin. The Sabine Peninsula is an exception to this, as surface strata are part of the Sverdrup Basin. The geology of the Sabine Peninsula consists of deformed Late Carboniferous to Paleocene sandstone, siltstone, shale, and minor amounts of carbonate. Additionally, evaporitic rocks are exposed in two depocenters on northern Sabine Peninsula—the Barrow and Collingwood domes, which consist of deformed anhydrite and gypsum. The strata of the Sverdrup Basin succession on Melville Island were deformed into a series of folds, including the Murray Harbour syncline in the northern part of the peninsula and the Drake Point anticline and the Maryatt Point syncline to the south (Harrison, 1994) (Fig. 1).

SEISMIC DATA SET AND PROCESSING
During a 1981 to 1985 phase of petroleum exploration, companies drilled 52 wells on Melville Island and surrounding waters (22 of which were on Sabine Peninsula) and acquired 3,400 line-kilometres of onshore seismic-reflection data (Fig. 2). Three separate gas fields were discovered in the Sabine Peninsula area: Drake Point, Hecla, and Roche Point. Feasibility studies for the development of the gas fields were conducted in the early 1980s; however, due to low gas prices and the lack of gas markets, the gas fields on Melville Island (and elsewhere in the Canadian Arctic) were not developed (Harrison, 1995).

Data access was obtained through a Memorandum of Understanding signed in 1997 by the Geological Survey of Canada (GSC), Panarctic Oils, the Arctic Islands Exploration Group, and the Offshore Arctic Exploration Group (joint venture parties). The data sets consist of original land seismic-reflection field tapes transferred from 21-, 7-, and 9-track media. Data were collected using a dynamic charge of 20–30 kg per shot at about 20 m below the surface. Shot-point spacing ranged from 67 m to 300 m, the shorter spacing being used for most surveys. The majority of the seismic-reflection data were recorded using 48- or 96-channel systems. Channel stations were separately deployed using nine receivers spaced at about 6 m and station intervals varying from 50 m to 70 m. The common-midpoint multiplicity of the data sets range from single to 12-fold coverage. The most common recording length was 6 s.

The processing consisted of these main steps: 1) principal component decomposition was used to remove both coherent and random noise; 2) data were migrated utilizing poststack Kirchhoff migration; and 3) seismic bandpasses were extended to increase vertical resolution (Claprood et al., 2011; Duchesne et al., 2012).

Velocity model
A 3-D velocity model was built using about 1300 km of linear seismic data (78 lines) and 13 wells spread over an area of about 2800 km² (Fig. 2). The velocity model was then used for poststack migration processing and to correct seismic horizon surfaces from time to depth. The primary assumption behind the velocity model is that the coherent high-amplitude reflectors that were picked to build the model correspond to important acoustic impedance contrasts caused by significant and abrupt velocity changes. This assumption was confirmed by using seismic picks to well sonic logs (Duchesne et al., 2012). The geostatistical approach of kriging with an external drift (KED) was applied to both the reflection time of the picked seismic horizons and time-depth pairs derived from check shot data to compute the 3-D velocity field. Kriging interpolates values between the known positions based on weighted spatial correlations. The KED technique was specifically developed for the integration of seismic data into the kriging process where the number of wells is insufficient for the computation of adequate depth statistics (Hass and Dubrule, 1994). Hence, it uses the information provided by the time horizon picks to improve estimates where depth control is sparse. For seismic migration, root mean squared (RMS) velocity values are first estimated by KED and then time-depth conversion of seismic horizon surfaces, mapped as important velocity boundaries (Duchesne et al., 2012). Then, once the approximate depths of the surfaces are known, the interval velocities (V_{int}) for all time intervals delimited by two consecutive horizons is computed for

$$V_{int} = \frac{\Delta z}{\Delta t}$$

where Δz and Δt are the depth and time intervals between two successive horizons i . Once V_{int} is obtained the RMS velocity (V_{rms}) is calculated using

$$V_{rms} = \sqrt{\frac{\sum_{i=1}^N V_{int}^2 \Delta t_i}{\sum_{i=1}^N \Delta t_i}}$$

in which N is the total number of horizons and Δt_i is the sum of all time intervals.

SEISMIC INTERPRETATION AND VISUALIZATION METHODS
Processed seismic lines were loaded into IHS Kingdom[®] seismic and geological interpretation software. Prominent seismic-reflection horizons, tied to well formation-log information, were manually correlated. Seed points were generated at seismic line intersections, thereby permitting the interpretation of adjacent lines.

The map would benefit from a detailed structural interpretation; however, confidence of this interpretation is minimized due to minor vertical offsets (about 0.1 s) attributed to faulting and the large line spacing. These reflections are readily identified across faults despite offset.

Time-structure maps of the key seismic horizons were computed using universal kriging. Universal kriging permits the interpolation of a nonstationary, random field by adding a term in the kriging equation that accommodates any linear trends present in a scattered point set (Chiles and Delfiner, 1999). Given that all picked horizons showed a strong linear trend for time versus depth over distance, universal kriging provided the best fit to the picked horizons.

TIME TO DEPTH CONVERSION
All time surfaces were converted to depth using the following procedure. First V_{rms} of the 3-D velocity model are calculated using Dix equation:

$$V_{int} = \left[\frac{V_{rms}^2(t_n) - V_{rms}^2(t_{n-1})}{t_n - t_{n-1}} \right]^{1/2}$$

where t is the zero-offset arrival time of the n th reflection. Interval limits corresponded to seismic horizons that are picked and tied to geological interfaces. Then V_{int} are entered from the velocity model along picked horizons. Velocity maps are then computed using Universal kriging at a cell size of 250 m. Finally, the time-structure surfaces of the various seismic horizons are converted to depth (z) using

$$Z = \frac{g}{2} t^2$$

Because the depth-conversion process is a function of the velocity model, the lateral extent of depth maps is confined to the lateral extent of the model. The final depth-structure maps were imported into ArcGIS for visualization using the Arc extension Team-GIS Bridge.

UNCERTAINTY
Quantifying the uncertainty of seismic subsurface maps is difficult since several sources of data, each with their unique level of uncertainty, are used in the map generation. Sources of error may arise from limitations in acquisition, processing, and interpretation. Moreover, seismic data are collected remotely and the images they provide are derived from generalized mathematical and physical concepts. The resulting processed seismic lines are a simplification that increase the uncertainty because of obstacles to source and receiver deployment, and effect of direction of shooting on data quality (Sherriff and Gokturt, 1995). Processing methods that increase the uncertainty include gaps in coverage, inaccurate velocity analysis, and inappropriate parameter determination.

More specifically to this data set, errors may have also been introduced by the velocity model and the ability to form time slices to seismic horizons. The velocity model represents an estimation of the velocity fluctuations for which the accuracy depends on the number of wells and the good fit between time picks and corresponding depths at the well locations. A regression analysis shows that time picks and their corresponding depths at the wells have a strong linear ($r = 0.98$), meaning that the use of time picks as the external drift in the kriging strategy is justified and suitable. Nevertheless, the uncertainty of the velocity model increases when the distance between the well and any points where velocity is predicted exceeds the range of the variogram expressing the spatial dependence of the velocity. In this study, the range of the variogram is between 6.5 km and 94 km. The ability to form time slices to seismic horizons relies on the successful use of well sonic and density logs, since it is the contrast between the product of these properties for two successive geological layers that generates reflections recorded in seismic exploration. Formation logs used in this study are from Dewing and Embry (2007), for which they mainly utilized gamma-ray logs to position the upper limit of the formation in depth. Thus errors may have been introduced by projecting the formation tops on seismic sections recorded in time.

TIME- AND DEPTH-STRUCTURE DATA DISPLAY
The time- and depth-structure data shown on this map were gridded at a cell size of 250 m using Universal kriging. Each map presents a grid with a stretched colour ramp at 20% transparency. Time contours generated from the time-structure grids are shown in black at 50 m interval, whereas depth contours derived from the depth-structure grid are presented at 100 m intervals.

SANDY POINT MAP DESCRIPTIONS
The Middle Jurassic Sandy Point Formation is composed of interbedded sandstone, siltstone, and shale (Embry, 1984; see also Fig. 3). The lower boundary of the Sandy Point Formation is in gradational contact with the underlying Jameson Bay Formation. In contrast, the contact with the overlying McConnell Island Formation is typically disconformable (Harrison, 1995). Formation-log data indicate that the top of the Sandy Point Formation was encountered in all wells on the Sabine Peninsula. The formation was consistently observed following the Jameson Bay Formation and was always overlain by the Rigney Formation, as exposed to the McConnell Island Formation (Dewing and Embry, 2007).

The thinned Sandy Point Formation reflection extends from the narrowest part of the peninsula near Eldridge and Shearard bays to the axis of the Murray Harbour syncline. The data gap west of Eldridge Bay marks the location of Barrow Dome. Two-way traveltimes increase northward from 130 ms to 197 ms, or from 422 m to 2918 m. Generally the slope of the horizon varies from 0 to 2°. The highest slopes, near 0°, are observed between the Drake Point anticline and the Barrow Dome, aligned roughly parallel to the axis of the Murray Harbour syncline. Steep slopes are also observed near the southern limit of the horizon. The primary slope azimuth of the horizon is to the north with the exception of the area between the axis of the Drake Point anticline and Maryatt Point syncline where the surface-tops are oriented to the centre of Sabine Peninsula.

ACKNOWLEDGMENTS
The authors would like to thank J. Dietrich and B. MacLean (GSC Calgary) for their technical reviews that improved the overall quality of the maps. IHS is acknowledged for providing Kingdom 8.8 seismic interpretation software.

REFERENCES
Chiles, J.-P., and Delfiner, P., 1999. Geostatistics: Modeling Spatial Uncertainty, Wiley Series in Probability and Statistics, Wiley, New York, 734 p.
Claprood, M., Duchesne, M.J., and Gosselin, E., 2011. A geostatistical approach for 2-D seismic velocity modelling. Geological Survey of Canada, OpenFile 7045, 21 p. doi:10.4095/290551
Dewing, K. and Embry, A.F., 2007. Geological and geochemical data from the Canadian Arctic Islands, Part I: Stratigraphic logs from Arctic Islands' oil and gas exploration basins. Geological Survey of Canada, Open File 5442, 133-ROOM. doi:10.4095/23386
Duchesne, M.J., Claprood, M., and Gosselin, E., 2012. Improving seismic velocity estimation for 2-D poststack time migration of regional seismic data using kriging with an external drift. The Leading Edge, v. 31, p. 1156–1166.
Embry, A.F., 1984. The Wilkes Point Group (Lower–Upper Jurassic), Sverdrup Basin, Arctic Islands, in Current Research, Geological Survey of Canada, Paper 84-15, p. 299–303. doi:10.4095/1668
Embry, A. and Beauchamp, B., 2008. Sverdrup Basin: In Sedimentary Basins of the World, ed. K.J. Holz, Volume 5, The Sedimentary Basins of the United States and Canada, Elsevier, Amsterdam, The Netherlands, p. 617–671.
Harrison, J.C., 1994. Melville Island and adjacent smaller islands, Canadian Arctic Archipelago, District of Franklin, Northwest Territories. Geological Survey of Canada, Map 1844A, scale 1:250 000. doi:10.4095/20377
Harrison, J.C., 1995. Melville Island's salt-based fold belt. Arctic Canada. Geological Survey of Canada, Bulletin 472, 344 p. doi:10.4095/20375
Hass, A. and Dubrule, O., 1994. Geostatistical inversion – a sequential method of stochastic reservoir modeling constrained by seismic data. First Break, v. 12, p. 951–959.
Sherriff, R.E. and Gokturt, L.P., 1995. Exploration Seismology. Cambridge University Press, New York, New York, 628 p.

Recommended citation
Brake, V.I., Duchesne, M.J., Dewing, K., Claprood, M., Gosselin, E., and Brent, T.A., 2013. Time- and depth-structure map, Sandy Point Formation, Sabine Peninsula, Melville Island, Nunavut-Northwest Territories. Geological Survey of Canada, Canadian Geoscience Map 164, scale 1:200 000. doi:10.4095/293088

CANADIAN GEOSCIENCE MAP 164
TIME- AND DEPTH-STRUCTURE MAP
SANDY POINT FORMATION
Sabine Peninsula, Melville Island
Nunavut-Northwest Territories